

Directed Energy Interception of Satellites

Harrison She^{a,b,*}, Will Hettel^b, Phillip Lubin^b

^a*Electrical and Computer Engineering and Physics Departments, University of Auckland, Auckland 1010, New Zealand*

^b*Physics Department, University of California, Santa Barbara, CA USA 93106-9530*

Abstract

High power earth and orbital-based directed energy (DE) systems pose a potential hazard to Earth orbiting spacecraft. The use of very high power large aperture DE systems to propel spacecraft is being pursued as the only known method to achieve relativistic flight in our NASA Starlight and Breakthrough Starshot programs. In addition, other beamed power mission scenarios, such as orbital debris removal and our NASA program using DE for powering high performance ion engine missions, pose similar concerns. It is critical to quantify the probability and rates of interception of the DE beam with the approximately 2000 active Earth orbiting spacecraft. We have modeled the interception of the beam with satellites by using their orbital parameters and computing the likelihood of interception for many of the scenarios of the proposed systems we are working on. We are able to simulate both the absolute interception as well as the distance and angle from the beam to the spacecraft, and have modeled a number of scenarios to obtain general probabilities. We have found that the probability of any active satellite, including its orbital position uncertainty, intercepting our beam during any of our many mission scenarios is extremely low ($\approx 10^{-4}$). The outcome of this work gives us the ability to predict when to energize the beam without intercept, as well as the capability to turn off the DE as needed for extended mission scenarios. As additional satellites are launched, our work can be readily extended to accommodate them by adding their orbital parameters to our database. Our work can also be used to predict intercept of astronomical adaptive optics guide-star lasers as well as any general

*Corresponding author
Email address: hshe55@gmail.com (Harrison She)

laser use.

Keywords: NASA Starlight, Breakthrough Starshot, directed energy, laser propulsion, satellites, situational space awareness

1. Introduction

1.1. Background

Directed energy systems are used routinely in astronomical application for laser guide-star excitation and for spacecraft laser communication. These systems typically have powers of 1–100 watts with sub-meter apertures. Larger scale directed energy systems have been proposed as a method of achieving relativistic flight (Bible et al., 2013; Hughes et al., 2014; Brashears et al., 2015; Lubin, 2016) to allow the first interstellar missions and rapid interplanetary transit. These DE systems are being actively pursued as a part of our NASA Starlight program, where a large aperture (1–10 kilometer diameter) phased array with multi GW power levels (Lubin, 2016). The derivative Breakthrough Starshot program uses the same technology, but focuses on the wafer-scale spacecraft and the ground-based array option. Laser systems have also been considered to characterize and intentionally remove orbital space debris in recent years (Lejba et al., 2018; Wang et al., 2016; Hou et al., 2016). In all of these cases, the DE beam has sufficient flux to cause damage to active Earth-orbiting satellites, which may be inadvertently illuminated.

To be able to accurately simulate such scenarios, it is imperative that the orbits of the satellites are determined accurately in order to predict when they may potentially intercept the beam. Space Situational Awareness (SSA) is concerned with the monitoring of the many Earth-orbiting bodies. Such programs are run both by the United States (NASA and DoD) and the European Space Agency (ESA). These programs involve the observation of the space environment, and the identification and tracking of space objects in that environment for international safety and security (Rovetto and Kelso, 2016). Crucially, SSA data from the North American Aerospace Defense Command (NORAD) can be acquired through Space Track, or an orbital body bulletin system

called CelesTrak (Kelso, 2017). This data aids in the tracking and ephemeris generation of satellite bodies in orbit around the Earth by providing two-line element sets (TLE) which encode a list of orbital elements to predict the position of each Earth-orbiting object at a specific time, allowing us to determine the probability of an interception.

1.2. Motivation

We use TLEs to simulate, analyze, and evaluate the frequency and duration of potential intercepts with the DE beam, as well as the distance by which an active satellite will miss the beam, when energized from a given location, at a given direction (both celestial and terrestrial) and time. Previously, the prediction of the orbits of satellites for beam intercept purposes was left to agencies that would give a “go/no-go” response, which is not adequate for understanding the operational implications of a system such as ours, nor does it allow for the precise orbital information necessary for an understanding of required optical sidelobe suppression. We use the term “intercept” to generally refer to the beam crossing the estimated position of the satellite including its positional uncertainty. Gating the DE off during all intercepts will ensure that no satellites are illuminated. The positional uncertainty of satellites is typically on the scale of kilometers and is thus vastly larger than the physical satellite. The actual probability of direct illumination of the satellite with the beam is significantly lower; we return to this later. Our interception calculations allow us to answer a number of questions including:

- How likely is a DE beam to intercept an active satellite, including its orbital uncertainty, during any given mission?
- How many satellites are likely to be intercepted by the DE beam for a given mission scenario?
- How many times, and for what duration, will the DE have to be gated off, and hence what is the transmission proportion that is likely to be achieved for a given DE mission?

Simulation of such outputs allows us to gauge the feasibility of a number of future directed energy missions, such as those proposed by Lubin (2016). These missions can

vary in total DE beaming duration from hundreds of seconds to several years. Shorter DE exposure missions include the proposal to accelerate ultra-light wafer spacecraft to relativistic velocities to reach Alpha Centauri. Longer DE exposure missions include, but are not limited to, continuous DE propulsion of larger scale payloads to closer range targets such as Mars, as well as missions to the moon or other planets. The results obtained from this research can also be applied to adaptive optics applications and other beamed power applications.

This paper discusses the design and development of a DE array and satellite ephemeris interdiction simulator. This simulator reads TLE objects from an online satellite catalog and subsequently calculates the ephemerides of active satellites that may be damaged during DE transmission. With the aid of the PyEphem library, which provides useful generic astronomical calculation functions, the aforementioned ephemerides can subsequently be utilized to simulate orbital motion (Rhodes, 2008). These, in conjunction with laser array model parameters, can be used to calculate potential intercepts with the DE beam. The simulator program allows the user to input a specific laser array site, a pointing target (right ascension, declination), a beam diameter, and start and end times for each simulation. With these parameters, the program calculates the total interception time, the total time the DE beam can transmit, and the distance (in linear and angular terms) between the DE beam and each satellite on the array's horizon. The program also includes a job scheduler that can be used to run multiple simulations in order to rapidly evaluate a multitude of potential mission scenarios that may arise.

2. Analytical approximation

We can approximate the laser-satellite intercept probability by assuming that the satellite distribution is spatially random at each altitude. We assume that satellites are “points” with an error “sphere” due to position determination uncertainty and allow for either a diverging or converging beam, with laser array (and hence beam) diameter d . For simplicity we assume the Earth is perfectly spherical and the satellite orbits are circular.

It is natural to expect that the number of interceptions with the DE beam should be small, since the density of Earth-orbiting spacecraft is extremely low. In fact, even the greatest density altitudes have just one object per 10 billion km² (Finkleman, 2014).

Definition of Variables

R_{\oplus} = radius of Earth

h = height of satellite above sea level

$v(h)$ = speed of satellite at height h

δ_{sat} = diameter of satellite position uncertainty

d_{sat} = actual size of satellite $\ll \delta_{\text{sat}}$

d = diameter laser optics

$\theta_{1/2}$ = laser divergence or convergence half-angle

$n_{\text{int-inst}}(h)$ = instantaneous number of beam intercepts with a single satellite at height h (equal to the probability that the beam will intercept a particular satellite at a given time)

n = total number of satellites

$N_{\text{int-inst}}$ = instantaneous number of beam intercepts with all satellites

$t_{\text{int-inst}}(h)$ = worst-case duration of single satellite beam crossing including satellite position uncertainty

$t_{\text{int-sat}}(h)$ = worst-case duration of single satellite beam crossing not including satellite position uncertainty ($\delta_{\text{sat}} = 0$)

$\frac{\delta n_{\text{int}}}{\delta t}(h)$ = number of single satellite intercepts per unit time

$\frac{\delta N_{\text{int}}}{\delta t}$ = total number of satellite intercepts per unit time

2.1. Intercept Probability

At the time of writing this paper, the full catalog of TLEs retrieved from the Space Track database consisted of 16776 satellite elements, most larger than 10 cm diameter. These elements comprise unclassified active and inactive satellites, as well as satellite

debris. For our purposes, we are only concerned with the 1783 satellite segments that are active (we do not worry about inactive satellites or debris). It is important to also note that at least 100 new satellites are launched into space each year (which will increase in the future), and hence it is important to update the TLE catalog used on a regular basis to include any new satellites (Finkleman, 2014).

Using PyEphem, the satellite altitudes from sea level have been calculated at an arbitrary point in time (midnight 2018/2/15), and plotted as a distribution seen in Fig. 1. From this plot, if we assume that most orbits are roughly circular (the median eccentricity of all 16776 TLE elements is 6×10^{-3} , as calculated using the same TLE data), we can see that most satellites fall into either the Low Earth or Geostationary orbital regimes.

In order to predict the probability of intercepting any satellite at a given time, we can use a simplified physical model to estimate approximate figures for our simulation. The simulation can also provide a means of validation for our model.

Let us assume that the Earth is a perfect sphere with a radius of 6371 km and we aim the DE beam in the zenith direction (directly upwards). If using the SGP4 model, which is used by PyEphem, the satellites deviate from their idealized orbits described by their TLE files by 1–3 km per day. We can use this information to model the tolerance (intercept volume) of each satellite as a 6 km diameter sphere, therefore setting $\delta_{\text{sat}} = 6$ km. We assume that the TLEs can be updated on a daily basis so δ_{sat} does not increase with time. The DE beam can be modeled as a cone extending from Earth to a geocentric sphere with radius $R_{\oplus} + h$.

With this we can model the probability of any single given satellite hitting the beam as the ratio of “intercept area” (shown in Fig. 2) to the total area of the geocentric sphere:

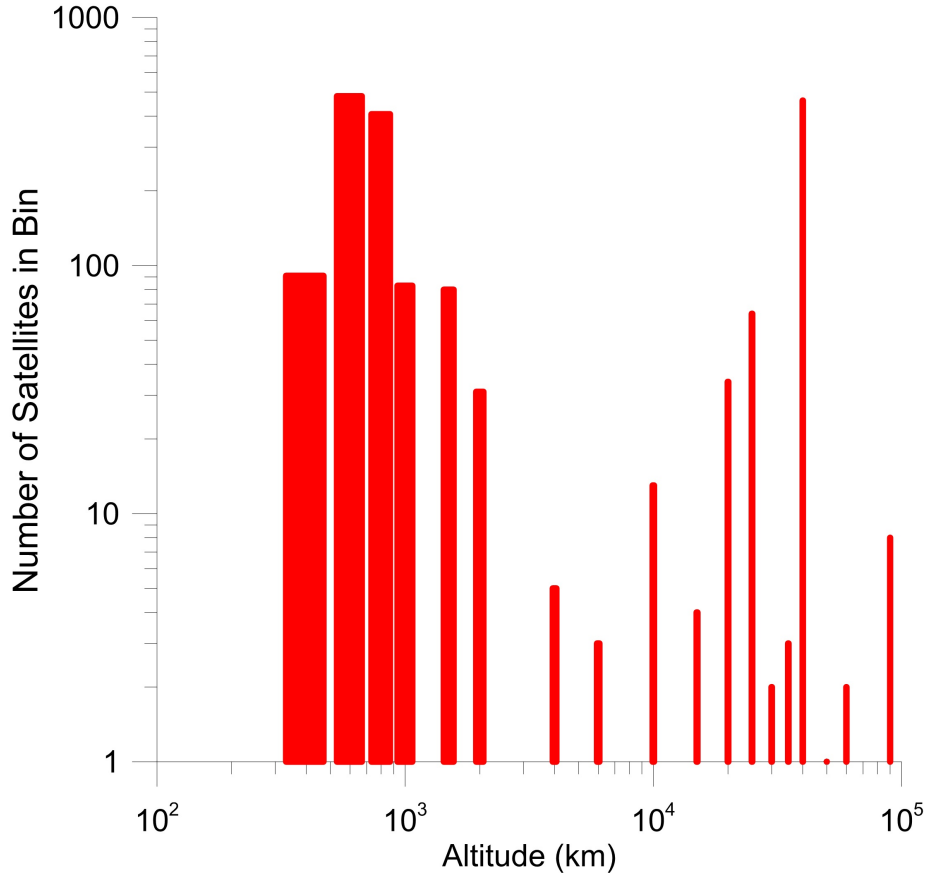


Figure 1: The distribution of 1783 active satellite altitudes at a given time. Most satellites fall into either Lower Earth Orbits (LEO) or Geosynchronous Orbits (GEO).

$$n_{\text{int-inst}}(h) = \frac{A_{\text{Intercept}}}{4\pi(R_{\oplus} + h)^2} \quad (1)$$

$$= \frac{\pi[d + 2h\theta_{1/2} + \delta_{\text{sat}} + d_{\text{sat}}]^2/4}{4\pi(R_{\oplus} + h)^2} \quad (2)$$

$$= \frac{[d + 2h\theta_{1/2} + \delta_{\text{sat}} + d_{\text{sat}}]^2}{16(R_{\oplus} + h)^2}. \quad (3)$$

A plot of $n_{\text{int-inst}}$ as a function of h is shown in Fig. 3. By summing $n_{\text{int-inst}}$ for n satellites, we find the probability that the beam will intercept any satellite at the given

time is

$$N_{\text{int-inst}} = \sum_{i=1}^n \frac{[d + 2h_i\theta_{1/2} + \delta_{\text{sat}} + d_{\text{sat}}]^2}{16(R_{\oplus} + h_i)^2}. \quad (4)$$

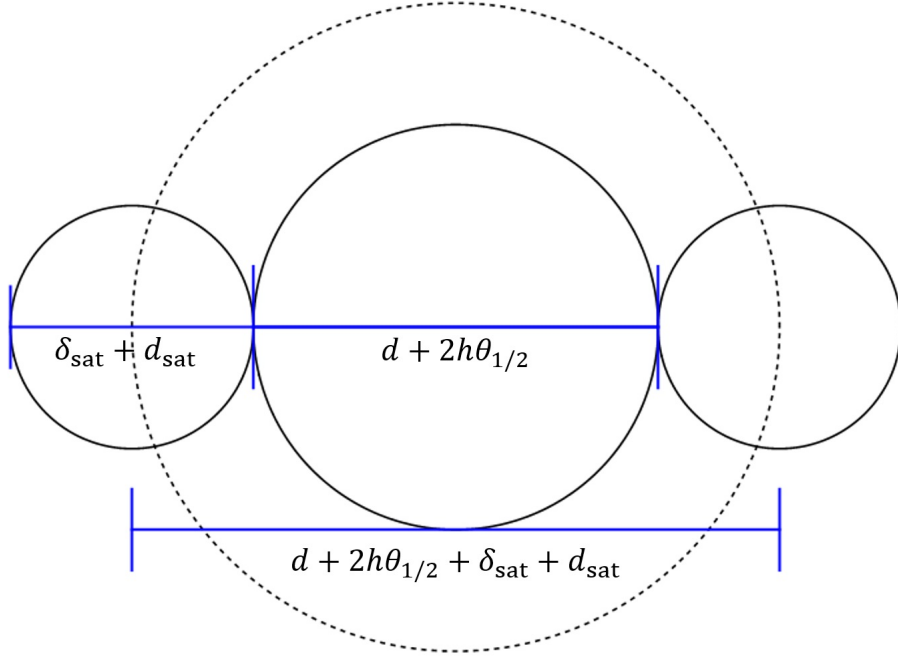


Figure 2: A model showing a DE beam (center) and two edge cases for intercepts (sides). An intercept is counted if the coordinate of satellite according to a TLE file (located at the center of the satellite’s error sphere) is within $(\delta_{\text{sat}} + d_{\text{sat}})/2$ of the edge of the beam, which ensures that all cases that a satellite may be illuminated are accounted for. This condition creates an effective “intercept area” equal to that of a circle of diameter $d + 2h\theta_{1/2} + \delta_{\text{sat}} + d_{\text{sat}}$. Intercepts are counted when TLE files report coordinates that are within this area.

We now assume that the diameter of the satellite and the laser half-angle are negligible ($d_{\text{sat}} = \theta_{1/2} = 0$) and calculate $N_{\text{int-inst}}$ for a laser array with $d = 10$ km and $\delta_{\text{sat}} = 6$ km and for $n = 1783$. We are justified in setting $\theta_{1/2} = 0$ because proposed missions require focusing at high altitude, so a significant divergence or convergence will not be expected. Furthermore, the half-angle due to diffraction of the 10 km laser array of 1064 nm wavelength proposed by Lubin (2016) is on the order of 10^{-10} radians

and is thus negligible compared to d/h and δ_{sat}/h .

We then have

$$N_{\text{int-inst}} = 3.9 \times 10^{-4}. \quad (5)$$

Therefore, from this result, we can see that even if no specific precautions are taken, the likelihood of an intercept in this conservative configuration is less than 10^{-3} . Note that the likelihood of a satellite actually being illuminated by the beam is smaller by a factor of $(\frac{d+d_{\text{sat}}}{d+\delta_{\text{sat}}})^2$ (≈ 0.4 for $d = 10$ km and $\delta_{\text{sat}} = 6$ km), because the true diameter of the satellite is d_{sat} as opposed to δ_{sat} . It should also be noted that the effective diameter of the beam at altitude will often be less than d (depending on focusing requirements for missions), further reducing the probability of illumination. If we assume all satellites have a diameter of 3 m, we can find the actual area covering fraction of satellites in the sky by setting $d = \delta_{\text{sat}} = 0$:

$$N_{\text{int-inst}} = 1.4 \times 10^{-11} \quad (6)$$

for $d_{\text{sat}} = 3$ m and $n = 1783$. As we can see, the true covering fraction is incredibly small.

2.2. Satellite Beam Crossing Duration and Frequency

It is important to not only characterize the transmission ratio, but also to characterize the duration and frequency of events in which the DE must be gated off. We can calculate these quantities using the velocities of spacecraft. If we again assume that orbits are circular, we have

$$F_c = \frac{M_{\text{sat}} v(h)^2}{R_{\oplus} + h} \quad (7)$$

$$F_g = \frac{GM_{\text{sat}}M_{\oplus}}{(R_{\oplus} + h)^2} \quad (8)$$

$$\text{setting } F_c = F_g \quad (9)$$

$$v(h) = \sqrt{\frac{GM_{\oplus}}{R_{\oplus} + h}}. \quad (10)$$

A plot of v as a function of h is shown in Fig. 3.

We obtain the mean velocity of all satellites by summing their individual velocities and dividing by the number of satellites:

$$\bar{v} = \frac{1}{n} \sum_{i=1}^n \sqrt{\frac{GM_{\oplus}}{R_{\oplus} + h_i}} \quad (11)$$

$$= 6086 \text{ m s}^{-1} \quad (12)$$

for the 1783 satellites used from the TLE data available to us. The worst-case duration of an intercept will be when the expected position of the satellite passes through the center of the beam. Since it takes a full day for a satellite to deviate from its expected orbit by 3 km, we assume that the velocity described by the TLE file is approximately equal to that of the satellite. We can thus assume that the distance traveled by the satellite during $t_{\text{int-inst}}$ is the same as that of its error sphere. We calculate $t_{\text{int-inst}}$ for a stationary DE beam with $d = 10$ km and $\theta_{1/2} = 0$, and a satellite with $\delta_{\text{sat}} = 6$ km and $d_{\text{sat}} = 0$ moving at average velocity to be

$$t_{\text{int-inst}}(h, \bar{v}) = \frac{d + 2h\theta_{1/2} + \delta_{\text{sat}} + d_{\text{sat}}}{\bar{v}} \quad (13)$$

$$= 2.63 \text{ s.} \quad (14)$$

Figure 3 shows $t_{\text{int-inst}}$ as a function of h . We will now calculate the number of intercepts with a given satellite per unit time. This will be equal to the area swept out by the satellite-laser system per unit time, divided by the area of the geocentric sphere of radius $R_{\oplus} + h$:

$$\frac{\delta n_{\text{int}}}{\delta t}(h) = \frac{(d + 2h\theta_{1/2} + \delta_{\text{sat}} + d_{\text{sat}})v(h)}{4\pi(R_{\oplus} + h)^2} \quad (15)$$

$$= \frac{4vn_{\text{int-inst}}(h)}{\pi(d + 2h\theta_{1/2} + \delta_{\text{sat}} + d_{\text{sat}})} \quad (16)$$

$$= \frac{4n_{\text{int-inst}}(h)}{\pi t_{\text{int-inst}}(h)}. \quad (17)$$

A plot of $\frac{\delta n_{\text{int}}}{\delta t}$ as a function of h is shown in Fig. 3. For all satellites, we can sum the number of intercepts per unit time to acquire a general intercept frequency:

$$\frac{\delta N_{\text{int}}}{\delta t} = \sum \frac{\delta n_{\text{int}}}{\delta t}(h) = \frac{4}{\pi} \sum_{i=1}^n \frac{n_{\text{int-inst}}(h_i)}{t_{\text{int-inst}}(h_i)} \frac{\delta N_{\text{int}}}{\delta t} = 0.000232 \text{ intercepts} \cdot \text{s}^{-1} \quad (18)$$

for $d = 10 \text{ km}$, $\theta_{1/2} = 0$, $\delta_{\text{sat}} = 6 \text{ km}$, $d_{\text{sat}} = 0$ and $n = 1783$. Thus, from this analysis we can see that the estimated intercepts per second is very low, and only once every 4310 seconds is it expected that a satellite will intercept the beam.

We will now calculate the worst-case intercept duration per unit time. For a single satellite, this is simply its intercept frequency multiplied by $t_{\text{int-inst}}$:

$$\frac{\delta n_{\text{int}}}{\delta t}(h)t_{\text{int-inst}}(h) = \frac{4}{\pi}n_{\text{int-inst}}(h). \quad (19)$$

For all satellites, we have

$$\sum \frac{\delta n_{\text{int}}}{\delta t}(h)t_{\text{int-inst}}(h) = \frac{4}{\pi} \sum_{i=1}^n n_{\text{int-inst}}(h_i) \quad (20)$$

$$= \frac{4}{\pi}N_{\text{int-inst}} \quad (21)$$

$$= 4.9 \times 10^{-4} \quad (22)$$

for $d = 10 \text{ km}$, $\theta_{1/2} = 0$, $\delta_{\text{sat}} = 6 \text{ km}$, $d_{\text{sat}} = 0$, and $n = 1783$.

2.3. Actual Satellite Beam Crossing Time

The typical size of satellites is on the order of meters, as opposed to the uncertainty of the orbital position, which is on the order of kilometers. For some applications, such as astronomical observations, the total duration that the satellite is exposed to the beam may be important. The actual worst-case beam crossing duration is

$$t_{\text{int-sat}}(h) = \frac{d + 2h\theta_{1/2} + d_{\text{sat}}}{v(h)}. \quad (23)$$

Plots of $t_{\text{int-sat}}$ as a function of h for various values of d are shown in Fig. 3. In these plots, the laser divergence half-angle due to diffraction is included as it is not negligible for small aperture diameters. We assume a circular aperture, which has $\theta_{1/2} = 1.22\lambda/d$.

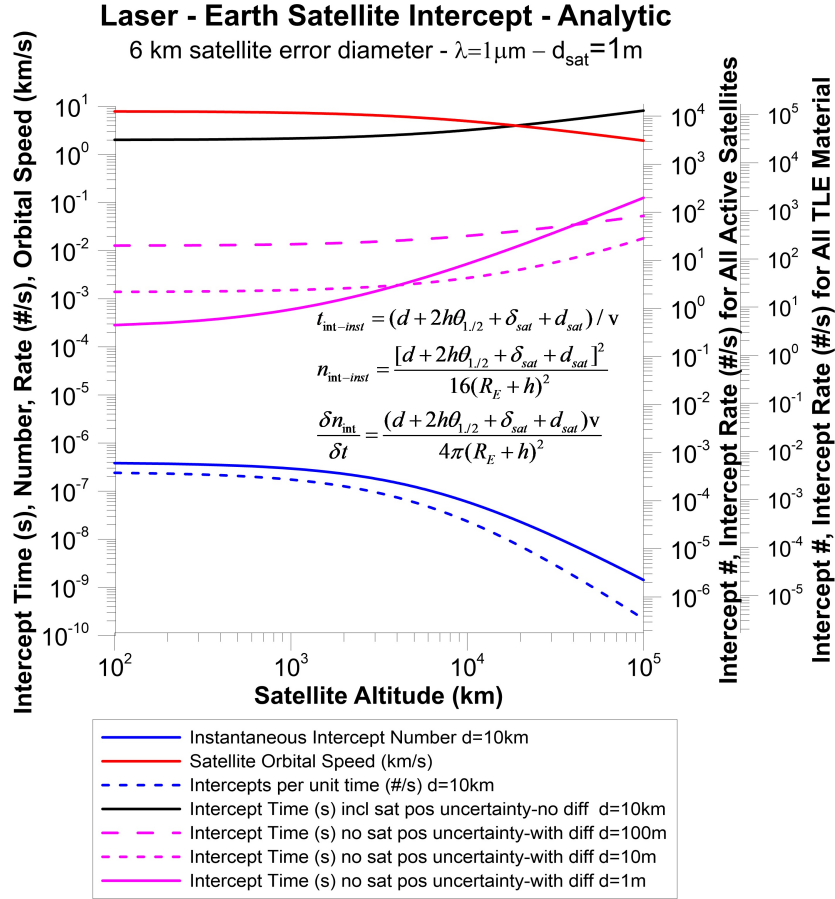


Figure 3: Intercept time, intercept rate, and orbital speed plotted as a function of satellite altitude. Here $\delta_{\text{sat}} = 6 \text{ km}$, $\lambda = 1064 \text{ nm}$, and $d_{\text{sat}} = 1 \text{ m}$. The solid blue line shows $n_{\text{int-inst}}$, the red line shows v , the dotted blue line shows $\frac{\delta n_{\text{int}}}{\delta t}$, the black line shows $t_{\text{int-inst}}$, and the magenta lines show $t_{\text{int-sat}}$ for various values of d . $n_{\text{int-inst}}$ and $\frac{\delta n_{\text{int}}}{\delta t}$ should be read on the right axes. v , $t_{\text{int-inst}}$, and $t_{\text{int-sat}}$ should be read on the left axis. The first right axis is scaled to account for all unclassified active satellites recognized by NORAD. The second right axis is scaled to account for all unclassified NORAD objects, including active and inactive satellites, debris, second stages, etc.

3. Directed energy safety concerns

In the event that the directed energy beam does in fact illuminate a satellite, it is important to note that for the mission to beam power to the moon, even for a 10 km laser array at the desired power of 100 GW, the flux is only approximately 1 kW/m^2 . This

flux is about the same as sunlight at sea level. Satellites will thus not be destroyed by the beam, however optical sensors may be adversely affected if exposed for extended periods of time. A flux of approximately 100 kW/m^2 warrants concern of thermal issues. For the interstellar mission to launch spacecraft to Alpha Centauri we can expect a much greater flux, as the beam needs to be focused on the wafer-scale spacecraft. Consequently, this is the most dangerous scenario for Earth-orbiting satellites. On the other hand, the interstellar case uses the DE beam for a much shorter period of time (at most 1000 s), so interceptions and instances where ground control needs to gate of the DE beam will be minimal.

Nonetheless, it is crucial that all directed energy missions obtain the authorization of the Laser Clearing House, as mandated by Department of Defense (DOD) Instruction 3100.11: Illumination of Objects in Space by Lasers (McKeon, 2016).

4. Methods

4.1. Dataset

In an attempt to answer our proposed research questions, a simulator program was written in Python using the PyEphem library (Rhodes, 2008). In order to model all the ephemerides of Earth-orbiting satellites, this library requires the parsing of TLEs for every unclassified tracked satellite we know about (see Fig. 4).

Satellite name																																																																				
Line no.	Satellite number	Class	International Designator	Epoch Yr	Epoch - Day of year (plus fractional portion of day)	1st time derivative of the mean motion (rev/day ²)	2nd Time Derivative of mean motion (rev/day ³ /6)	BSTAR drag term (E _r)	Eph	Elem set num	Chk sum																																																									
	Yr	Lchr	Piece			Sign	Sign	Sign																																																												
1	2 5 5 4 4 U		9 8 0 6 7 A	1 8 0 5 1	9 6 4 5 7 6 2 5	0 0 0 0 2 5 7 7	0 0 0 0 0 0 - 0	4 6 1 6 9 - 4	0		9 9 9 0																																																									
			Inclination (deg)	Right ascension of the node (deg)	Eccentricity	Arg of perigee (deg)	Mean anomaly (deg)	Mean motion (rev/day)	Revolution no. at epoch		Chk sum																																																									
2	2 5 5 4 4		8 1 . 6 4 1 6	2 3 8 . 1 0 8 9	0 0 0 3 4 3 7	1 1 7 . 8 4 7 8	3 5 7 . 3 2 6 1	1 5 . 1 5 4 1 2 5 9 1	2 1 0 0 4 4	0																																																										

Figure 4: An example of TLE set for the International Space Station (ISS)

These TLEs are 69 column, two-line elements that represent a given satellite and its orbital elements. The format of these TLEs was originally intended for 80-column

punch card inputs, and has now been adapted to ASCII text files. An example TLE of the International Space Station is shown in Fig. 4, with all the elements of each column of the TLE defined. It is important to note that the decimal point is implied for the second time derivative of mean motion, the BSTAR drag term, and the eccentricity. The yellow highlighted blocks indicate that these columns are always blank for parsing purposes (Kelso, 2018).

TLEs are fundamentally general perturbation element sets that contain mean values of orbital parameters, which are pre-processed by NORAD (North American Aerospace Defense Command) to remove periodic variations. Therefore, in order to use these TLEs to obtain accurate predictions, we must reconstruct the periodic variations in the appropriate manner, namely, in the exact same way that NORAD first removed these variations (Kelso et al., 1988; Osweiler, 2006). The PyEphem astronomical python library gives us the ability to do this, as it utilizes SGP4 (Standard General Perturbations Satellite Orbit Model 4) to compute the ephemeris of each satellite defined by a TLE.

Such data can be retrieved from the Space Track or the CelesTrak online bulletin board system, which both acquire these TLEs directly from NORAD. CelesTrak also groups sets of TLEs into logical categories such as low Earth orbit (LEO), geosynchronous orbit, scientific, communication, navigation, and more.

It is important to note that the SGP4 model is not the most precise method available to derive the ephemeris of satellites from TLEs. Indeed, there exists inherent limitations in using TLE files for any analysis, since the calculation accuracy is limited by the number of decimal places that orbital parameter fields can fit in the 69 column TLE. As a direct result, TLE data can only be accurate to approximately 1–3 km at the time of the epoch, and degrade as calculations are performed further from this date (Vallado et al., 2006; Rhodes, 2015; Finkleman, 2014). This uncertainty has been taken into account in both our analytical approximation and numerically simulated results.

The physical and mathematical method of how the ephemeris is derived from this

model is presented in detail in Sec. 4.2. In addition, how the ephemerides are subsequently processed in our simulation code is explained in Sec. 4.3.

4.2. Physics and Mathematics of Calculations

The SGP4 orbit propagator uses an analytic low-order solution to Newton's second law, giving a realistic model for gravitational potential and a dissipative atmospheric environment (Picone et al., 2005). This model is used for near-Earth satellites and was developed in 1970 by Ken Cranford (Lane and Hoots, 1979), and is a simplification of the more complex theory of Lane and Cranford, which uses a power density function for the atmosphere and a gravitational model from Brouwer's solution (Brouwer, 1959). Outlined below is a summary of the results deriving the position of a satellite from columns 09-63 of line 2 of each TLE, which use the following orbital elements at the Epoch: the mean motion (n_o), eccentricity (e_o), inclination (i_o), argument of perigee (ω_o), the longitude of ascending node (Ω_o), the mean anomaly (M_o), the first time derivative of the mean motion (\dot{n}_o), and the second time derivative of mean motion (\ddot{n}_o), to calculate the position and velocity vectors from the observer to a given satellite in the radial direction as \mathbf{r} and $\dot{\mathbf{r}}$, respectively, using the method used in Space Track (Kelso et al., 1988):

$$\mathbf{r} = r_k \mathbf{U} \quad (24)$$

$$\dot{\mathbf{r}} = \dot{r}_k \mathbf{U} + (r \dot{f})_k \mathbf{V}, \quad (25)$$

where

$$\mathbf{U} = \mathbf{M} \sin u_k + \mathbf{N} \cos u_k \quad (26)$$

$$\mathbf{V} = \mathbf{M} \cos u_k - \mathbf{N} \sin u_k \quad (27)$$

and

$$\mathbf{M} = \begin{pmatrix} M_x = -\sin \Omega_k \cos i_k \\ M_y = \cos \Omega_k \cos i_k \\ M_z = \sin i_k \end{pmatrix}$$

$$N = \begin{cases} N_x = \cos \Omega_k \\ N_y = \sin \Omega_k \\ N_z = 0 \end{cases}$$

$$r_k = r \left[1 - \frac{3}{2} k_2 \frac{\sqrt{1 - e_L^2}}{p_L^2} (3\theta^2 - 1) \right] + \Delta r$$

$$u_k = u + \Delta u$$

$$\Omega_k = \Omega + \Delta \Omega$$

$$i_k = i_o + \Delta i.$$

Symbols not defined here can be viewed alongside the complete derivation of these results from the Space-Track report in Appendix A (Kelso et al., 1988).

4.3. Simulations

4.3.1. Calculating total intercept duration

A single TLE can be read in through PyEphem’s `readtle()` function, which creates a body object for that satellite segment. Subsequently, these satellite objects are used to compute ephemeris, model the laser and calculate the intercepts. At a high level, this can be described in the following steps:

1. Retrieve all satellites orbital parameters as TLEs (Two-line element sets) from the Space Track database (NORAD).
2. Use `ephem.compute` to derive the position (altitude angle, azimuth angle, latitude, longitude, and elevation) for each satellite at a particular date and time.
3. Model the tolerance (intercept volume) of each satellite using the information that satellites deviate from their idealized orbits described by their TLEs by 1–3 km per day.
4. Model the intercept volume of an laser array of a certain diameter, situated on the Earth, pointing at a given target.
5. Calculate the time that the pointing target for the laser array is above the horizon, which equates to the “total effective beam time.”

6. Calculate the points of interception between satellites and the beam for a given start time and beaming duration.
7. Calculate the duration of each intercept and add these intervals together to calculate total intercept time, and hence the interception time fraction. It is important to note that here, an intercept is defined as the error sphere of the satellites having a non-zero overlap with the uncertainty of the beam.

For each scenario simulation, the configurable inputs of the program are given as follows:

- Laser array location (Defined by latitude & longitude)
- Laser pointing target (Defined by right ascension & declination)
- Starting date and time to energize beam
- Duration from initial beam on to beam off (s)
- Beam diameter (m)

The simulation then generates a list of the intercepts (which contain the position of the particular satellite and the date and time when they intercepted the DE beam) and then returns the total calculated intercept time and number of intercepts for the simulation. The in-depth program is summarized in Algorithms 1 and 2.

4.3.2. *Satellite distance calculation*

[†]The distance from the center of the beam to the expected position of the satellite, which we will call p , is calculated using a function (`calculateDistance()`) as follows. The user inputs the laser's latitude ϕ , the laser's longitude λ , and the target's right ascension and declination which are then converted to its altitude angle α and azimuth angle β . PyEphem uses ϕ and λ to return the latitude ϕ_s , longitude λ_s , altitude angle α_s , azimuth angle β_s and elevation h above sea level of the satellite. First, the distance r_k from the laser array site to the satellite is calculated by the law of cosines:

$$r_k = (R_{\oplus} + h) \left[1 + \left(\frac{R_{\oplus}}{R_{\oplus} + h} \right)^2 - 2 \left(\frac{R_{\oplus}}{R_{\oplus} + h} \right) \cos \gamma \right]^{1/2}, \quad (28)$$

Algorithm 1 Calculating Number Of Intercepts And Total Intercept Time

```
LEO_ORBITAL_SPEED ← 7800 m s-1
satelliteUncertainty ← 6000 m
resolution ← 500
stepSize ← 1 s
effectiveBeamTime ← calculateEffectiveBeamTime(startTime, beamingDuration)
totalInterceptTime, numIntercepts ← calculateTotalInterceptTime(site, target, startTime, beamingDuration,
beamDiameter)
interceptFraction ← totalInterceptTime/effectiveBeamTime
```

```
function CALCULATETOTALINTERCEPTTIME(site, target, startTime, beamingDuration, beamDiameter)
```

```
  satellites ← readTLES(TLE)
  observer ← setup(site, target, startTime)
  interceptIntervals ← ∅
  for all satellite ∈ satellites do
    currentTime ← startTime
    intercepts ← ∅
    satellitePosition ← computePosition(observer, target)
    distanceToBeam ← calculateDistance(satellitePosition)†

    if distanceToBeam < (beamDiameter + satelliteUncertainty)/2 then
      intercept ← currentTime
      intercepts.add(intercept)
      numIntercepts ← numIntercepts + 1
    end if

    timestep ← distanceToBeam/(resolution × LEO_ORBITAL_SPEED)
    currentTime ← currentTime + timestep

    if ∃ intercepts then
      interceptInterval ← (intercepts[0], intercepts[intercepts.length - 1])
      interceptIntervals.add(interval)
    end if
  end for

  for all interval ∈ interceptIntervals do
    totalInterceptTime ← totalInterceptTime + interval
  end for

  return totalInterceptTime, numIntercepts
end function
```

Algorithm 2 Calculating Effective Beam Time

```
function CALCULATEEFFECTIVEBEAMTIME(startTime, beamingDuration)
    timeAboveHorizon  $\leftarrow$  0
    timeAbove30Degrees  $\leftarrow$  0
    currentTime  $\leftarrow$  startTime
    endDateTime  $\leftarrow$  startTime + beamingDuration

    while currentTime < endDateTime do
        pointingAltitude  $\leftarrow$  computePosition(observer, target)
        if pointingAltitude  $\in$  [0, 90] then
            timeAboveHorizon  $\leftarrow$  timeAboveHorizon + stepSize
        end if
        if pointingAltitude  $\in$  [30, 90] then
            timeAbove30Degrees  $\leftarrow$  timeAbove30Degrees + stepSize
        end if
        currentTime  $\leftarrow$  currentTime + stepSize
    end while

    return timeAboveHorizon, timeAbove30Degrees
end function
```

where R_{\oplus} is the radius of the earth and γ is the angle between the laser and satellite's radius vectors shown in Fig. 5. From the dot product in spherical coordinates, we have

$$\cos \gamma = \cos \phi_s \cos \phi \cos (\lambda - \lambda_s) + \sin \phi_s \sin \phi. \quad (29)$$

Next, the angle θ between the beam and the satellite (shown in Fig. 6) is used with r_k to calculate p . The computation of θ is similar to that of γ :

$$\cos \theta = \cos \alpha_s \cos \alpha \cos (\beta - \beta_s) + \sin \alpha_s \sin \alpha \quad (30)$$

$$(31)$$

$$\sin \theta = (1 - \cos \theta^2)^{1/2}. \quad (32)$$

Finally, the distance from the center of the beam to the expected position of the satellite is

$$p = r_k \sin \theta. \quad (33)$$

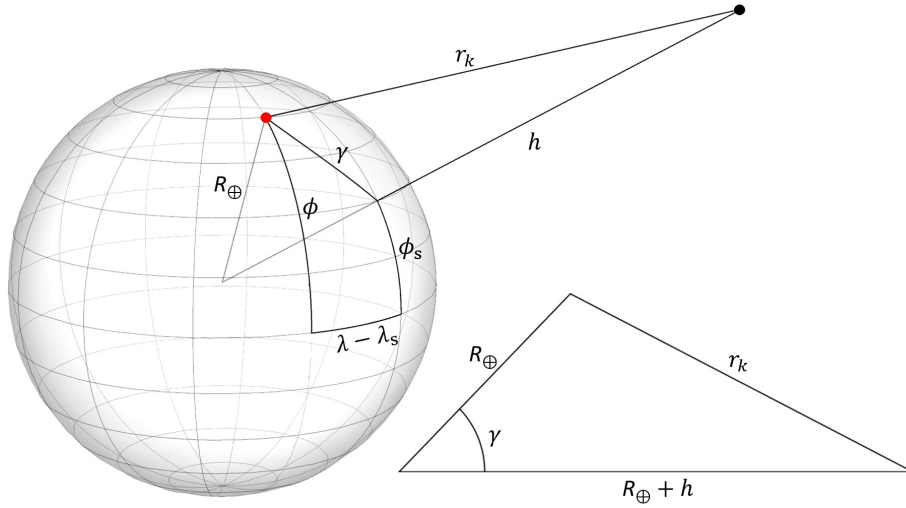


Figure 5: Left: A model of the Earth showing the locations of a laser array (red circle), a satellite (black circle), their coordinates, and the angle γ between them. r_k is the distance between the laser and satellite. Right: The law of cosines is used to calculate r_k using R_\oplus , h , and γ .

If p is within $(d + \delta_{\text{sat}})/2$, an intercept is counted. We neglect the size of the satellite and the laser half-angle for the reasons described in Sec. 2.1.

4.3.3. Time step error analysis

In computational simulations, there is naturally an error in output values due to the finite resolution of their calculations. In our case, this error originates from the size of the time step between data points. Our simulation uses a dynamic time step Δt equal to the distance p between the expected position of the satellite and the center of the beam divided by the speed of low-Earth orbital satellites (denoted as $v_{\text{LEO}} = 7800$ m/s) and scaled by a resolution number N_{res} :

$$\Delta t = \frac{p}{N_{\text{res}} v_{\text{LEO}}}. \quad (34)$$

The time resolution only plays a role when a satellite enters and exits the beam. The most extreme error in the measurement of intercept time that can occur is when the data points for the satellite's position are at the very edge of the intercept area. In

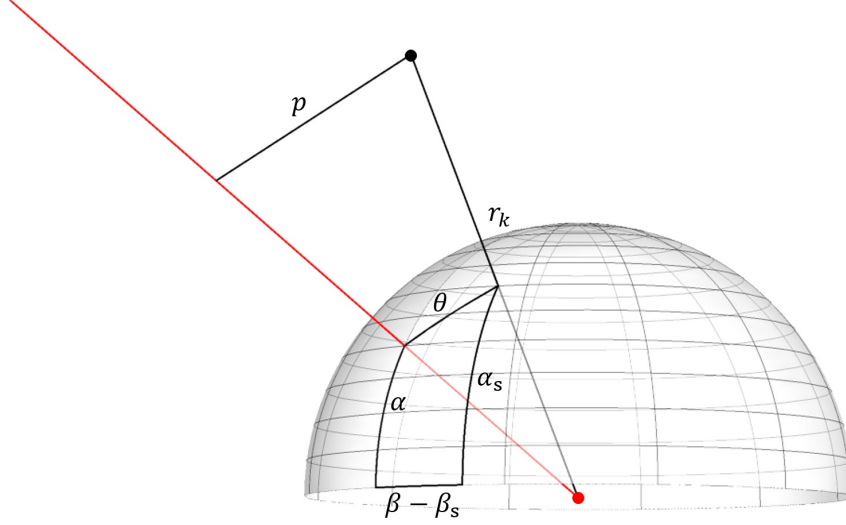


Figure 6: A celestial sphere centered at the location of the laser array (red circle), showing the altitude angle α and azimuth angle β of the beam, as well a satellite (black circle) with altitude angle α_s and azimuth angle β_s . θ is the angular displacement between the laser and satellite, r_k is the distance from the laser to the satellite, and p is the shortest distance from the satellite to the center of the beam.

this case,

$$p = \frac{d + \delta_{\text{sat}}}{2} \quad (35)$$

$$\Delta t = \frac{d + \delta_{\text{sat}}}{2N_{\text{res}}v_{\text{LEO}}}. \quad (36)$$

The error δt_{int} is

$$\delta t_{\text{int}} = 2\Delta t = \frac{d + \delta_{\text{sat}}}{N_{\text{res}}v_{\text{LEO}}}. \quad (37)$$

The total error in intercept duration for N_{int} number of intercepts is then

$$\delta T_{\text{int}} = \sum \delta t_{\text{int}} = N_{\text{int}} \frac{d + \delta_{\text{sat}}}{N_{\text{res}}v_{\text{LEO}}}. \quad (38)$$

The time resolution also produces an error in N_{int} , which we will call δN_{int} . The intercept time for some satellites may be less than Δt if their error sphere just clips

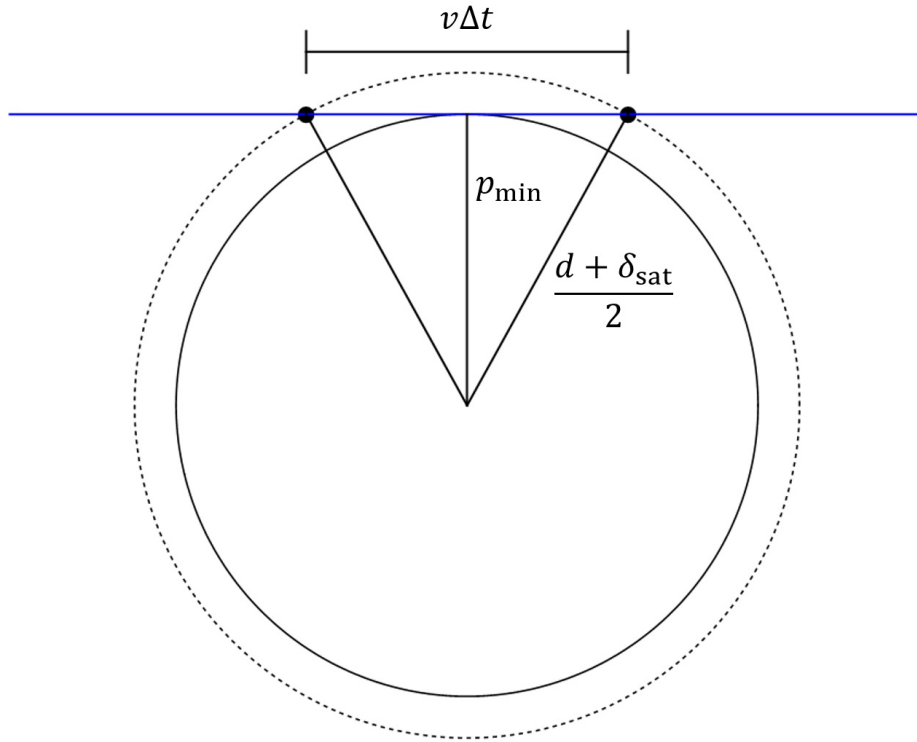


Figure 7: The intercept area as seen by the simulation (solid circle) is dependent on the time resolution. The dotted circle is the true intercept area shown in Fig. 2. The blue line represents a satellite's trajectory as described by its TLE file, and the black dots represent two consecutive calculations of its location separated by the time interval Δt . In this case, an intercept is not counted, even though the expected position of the satellite passes through the intercept area. Thus, the effective intercept area is that of a circle with a diameter $2p_{\min}$ (p_{\min} is the closest distance from the satellite's expected trajectory to the center of the beam) rather than $d + \delta_{\text{sat}}$.

the edge of the beam, in which case the simulation will not record an intercept. In the most extreme case, two data points are collected at $p = (d + \delta_{\text{sat}})/2$ before and after the expected trajectory of the satellite crosses the intercept area (see Fig. 7). This condition creates a new effective intercept area equal to the area of a circle with diameter $2p_{\min}$ rather than $d + \delta_{\text{sat}}$, where p_{\min} is the closest distance from the satellite's expected trajectory to the center of the beam. Using the satellite's speed v and assuming the

beam is stationary (which it will be on average), we have

$$p_{\min} = \frac{1}{2} \sqrt{(d + \delta_{\text{sat}})^2 - (v\Delta t)^2} \quad (39)$$

$$A_{\text{Intercept}} = \frac{\pi}{4} [(d + \delta_{\text{sat}})^2 - (v\Delta t)^2]. \quad (40)$$

The fractional change in n_{int} intercepts with a single satellite, which is equal to the fractional change in intercept area, is then

$$\frac{n_{\text{int}} - \delta n_{\text{int}}}{n_{\text{int}}} = \frac{(d + \delta_{\text{sat}})^2 - (v\Delta t)^2}{(d + \delta_{\text{sat}})^2} \quad (41)$$

$$\therefore \delta n_{\text{int}} = n_{\text{int}} \frac{(v\Delta t)^2}{(d + \delta_{\text{sat}})^2}, \quad (42)$$

where δn_{int} is the error in the number of intercepts with a single satellite. Using Eq. (36) to replace Δt , this error is

$$\delta n_{\text{int}} = n_{\text{int}} \frac{v^2}{(2N_{\text{res}}v_{\text{LEO}})^2}. \quad (43)$$

For all satellites, we have

$$\delta N_{\text{int}} = \sum n_{\text{int}} \frac{v^2}{(2N_{\text{res}}v_{\text{LEO}})^2} \quad (44)$$

$$\leq \sum n_{\text{int}} \frac{v_{\text{LEO}}^2}{(2N_{\text{res}}v_{\text{LEO}})^2} \quad (45)$$

$$= \frac{N_{\text{int}}}{4N_{\text{res}}^2}. \quad (46)$$

The above quantity is the highest expected error in number of intercepts with all satellites for a given simulation. The value for N_{res} was chosen so that it was in a regime where our results were invariant as a function of the time step size, to the reported accuracy. Our choice $N_{\text{res}} = 500$ is safely in this regime. Due to their dependencies on N_{res} , the results for number of intercepts converged much more rapidly than those for intercept duration, so in general $\delta N_{\text{int}} \ll 1$.

4.3.4. Calculating distances from beam to all satellites at a given instant

As another heuristic and useful tool to determine the probability of intercepting Earth-orbiting satellites, calculating the shortest distance from each satellite to the beam at a given distance was implemented. This was carried out for validation purposes as well as to give a clear idea of the distribution of distances of satellites from the beam for any given time, place and target. The algorithm pseudo-code is presented in Algorithm 3.

Algorithm 3 Calculate distance from beam to all satellites simulator

```
function CALCULATEDISTANCESNAPSHOT(site, target, time)
  satellites  $\leftarrow$  readTLEFile(TLEFile)
  observer  $\leftarrow$  setup(site, target, time)
  distances  $\leftarrow$   $\emptyset$ 

  for all satellite  $\in$  satellites do
    currentTime  $\leftarrow$  time
    satellitePosition  $\leftarrow$  computePosition(observer, target)
    if satellitePosition.altitude > 0 then
      distanceToBeam  $\leftarrow$  calculateDistance(satellitePosition, observer)†
      distances.add(distanceToBeam)
    end if
  end for

  return distances
end function
```

The shortest distance between the beam and a given satellite is calculated in Sec. 4.3.2. Refer to Fig. 6 for a geometric visualization. This calculation yields the distance from the expected position of the satellite to the center of the beam, not the worst-case minimum distance from the satellite to the edge of the beam. In other words, this distance should not be less than $(d + \delta_{\text{sat}})/2$ before the DE is gated off. Satellites that are under the horizon ($\alpha_s < 0^\circ$) or behind the laser array ($\theta > 90^\circ$) are ignored.

4.3.5. Scenario planning

In order to answer the research questions, a number of laser array base sites were chosen for the potential placement of a multi-element laser array that will be used in future missions. These sites are given in Table 1. The targets chosen pertain to specific

future proposed NASA missions and are tabulated in Table 2.

Table 1: Laser array base sites.

Laser Array Base Site	Location	Latitude (deg)	Longitude (deg)	Declin. range (deg)	Altitude (m)
Barcroft Station	Mono County, California	37.584	-118.237	[-22.417,97.584]	3100
ALMA	Atacama Desert, Santiago, Chile	-23.023	-67.755	[-83.023,36.977]	3158
Haleakala Observatory	Kula, Hawaii	20.710	-156.253	[-39.290,80.710]	3052
South Pole	Antarctica	-90.000	0.000	[-30.000,60.000]	2800

The laser array continuously tracks the specified target for the duration of the simulation, but can only activate when the target is above the horizon of the array. It is therefore important for any given mission to consider both the time when the beam is above the horizon, as well as the intercept fraction.

The first scenario that we are exploring through our simulations is the long-term interstellar mission to the Alpha Centauri system. Proxima Centauri is the nearest solar system to our own, being about 4.24 light years away. Proxima Centauri has at least one confirmed exoplanet (Proxima b). There may be other in the same system. Interstellar travel is extremely difficult and not feasible for humans to undertake. However, we can instead use “remote sensing” through lightweight electronic systems (i.e., wafer spacecraft) to allow for exploration across vast distances (Lubin, 2016).

In the mission proposed by Lubin (2016), it is shown through analysis that a 100 GW DE system can accelerate a wafer spacecraft that weighs 1 gram to 0.25c in a few minutes of laser illumination, reaching the Alpha Centauri region within about 20 years. This short acceleration time would potentially allow for hundreds of missions per day, or approximately one-hundred thousand missions per year. The ability to propel a multitude of spacecraft in large numbers means spreading the risk of failed missions over the constellation of spacecraft. This method of exploration can be reasoned about in a similar vein to the concept of an r-strategist organism in ecology. In ecology, an r-strategist is an opportunist that produces a large number of inexpensive offspring, which works very well in surviving in unknown and unstable environments (South-

wood et al., 1974). In our case, we are sending many spacecraft out, and can tolerate single spacecraft failures due to the large swarm strategy we would use.

Wafer-scale spacecraft are not the only type of payload to be explored. Heavier payloads can be accelerated through the same DE system, for rapid transit to closer targets such as the Moon, Mars, and Pluto. For example, in these regimes, a 100 kg payload may be accelerated to 0.01c, and a 10-ton payload potentially to over 1000 km/s. Since fuel is no longer an issue, and the directed energy propulsion system is on earth, such missions would become more cost-effective and more rapid to deploy.

Of particular importance in the shorter-term vision of Starlight are missions that involves using a DE beam to power high performance ion engines on the spacecraft allowing high mass interplanetary missions at modest speeds. These are not for relativistic flight applications but do allow much higher mass missions in the solar system. High mass tugs back and forth to the Moon or Mars are one example of this.

Table 2: Targets.

Target	Distance from Earth
Alpha Centauri A	4.367 ly
The Moon	384,400 km
Mars	54.6 million km
Pluto	7.5 billion km

Appropriate beaming durations and beam diameters were chosen for each simulation depending on the proposed scenario. For example, 1000 seconds was chosen for the Alpha Centauri target scenario, as this is a conservative upper-bound on the time that the directed energy must be energized in order to accelerate gram-scale wafercrafts to relativistic speeds. Other time periods include a 3-month duration for Mars, a 1-year period for the moon, and a 3-year period for Pluto. A 100 m beam diameter was chosen for the moon-based mission, whereas a 10 km diameter was chosen for all

other scenarios.

Each mission scenario was simulated for each of the four candidate laser array base sites to investigate the relative importance of the location of the laser array for any given mission. Simulations were run on a Desktop computer, with an Intel Core 2 Quad Q6600 CPU @ 2.40GHz, 8GB of RAM, and Windows 7 Ultimate edition.

5. Results

With the methodology established, we are subsequently able to carry out the simulations and measure a number of interesting results. For each simulation, the following results were calculated:

- *t desired* or the desired illumination time denotes the time we wish to keep the DE beam on from the starting date.
- *t above 0°* denotes the total time that the desired target is above the horizon (the total time we can aim the DE beam at the target without going through the Earth).
- *t above 30°* is a similar metric as above, except now only measures the time when the beam is 30° above the horizon when pointing at the target. At less than 30° above the horizon, atmospheric absorption and scattering of the DE become more significant, reducing the desired intensity of the beam at the target.
- *No. Int.s* represents the number of times that satellites have intercepted the beam during the mission simulation.
- *Int. duration* represents the total time that satellites have intercepted the beam during the simulation. It is important to note that we have ensured in our simulation (using an intercept interval merging algorithm), that two or more satellites intercepting the beam at the same time are not double-counted.
- The *Int. Fraction* represents the fraction of total time that satellites intercept the beam out of the time that the desired target is above the horizon ($Int. duration / t above 0^\circ$).

The start date and time of each simulation was set to March 20th, 2018 at midnight. The error bounds were set by use of the equations in Sec. 4.3.3.

5.1. *Alpha Centauri*

Simulations were run for a low mass (≈ 10 g) wafer scale spacecraft interstellar mission, targeting Alpha Centauri, using a beaming duration of 1000 seconds, a beam diameter set at 10 km (for a 100 GW DE beam), and only considering active satellites.

In general, the simulated interstellar cases with a 1000-second beaming duration did not yield an intercept. This is consistent with our analytic solution, as the number of intercepts per second was calculated at 0.000232 intercepts/second, which corresponds to, on average, 0.232 intercepts in 1000 seconds.

From this, it is evident that at any given location on Earth, there always must exist a window of at least 1000 seconds where the beam never intercepts any satellites. Therefore, the ability to launch these wafer satellites without the DE beam intercepting another active satellite (and therefore not needing to gate the DE beam off during the acceleration period) is highly likely.

5.2. *The Moon*

Simulations pertaining to missions to the the moon were conducted. These would be done primarily using much lower power (<100 MW) driving high performance ion engines. Since such missions are much closer and could be extremely frequent, we use beam diameter of 100 m and allow for continuous operation for a year and only consider active satellites. The results are tabulated in Table 3.

For the long-term lunar operations, it is critical that the transmission proportion be very high. This means that the beam should not be gated off for extended periods of time. As we can see from Table 3, this is overwhelmingly the case, with a intercept fraction ranging from just 6.06×10^{-5} to 2.66×10^{-4} . Note that the intercept fraction of the moon mission is an order of magnitude lower than that of the Mars and Pluto missions because of the decreased beam size (100 m rather than 10 km).

Table 3: Simulation: Moon.

Laser Array Base Site	t desired	t above 0°	t above 30°	No. Int.s	Int. duration	Int. fraction
Barcroft Station	1 year	180.338 days	89.423 days	$1528 \pm < 1$	$19.1 \pm < 0.1$ mins	7.34×10^{-5}
Atacama	1 year	181.914 days	110.780 days	$1358 \pm < 1$	$15.9 \pm < 0.1$ mins	6.06×10^{-5}
Haleakala	1 year	181.114 days	111.266 days	$1427 \pm < 1$	$16.8 \pm < 0.1$ mins	6.43×10^{-5}
South Pole	1 year	186.794 days	0 days	$4737 \pm < 1$	71.6 ± 0.1 mins	2.66×10^{-4}

Table 4: A sample distance snapshot simulation.

Satellite name	Distance (km)	Angular Disp. (deg)	Altitude (deg)	Azimuth (deg)	Elevation (km)
AEROCUBE 7C	78	9.03399	67.388	190.662	453
YAOGAN 4	225	15.65786	50.572	158.021	654
AEROCUBE 7B	303	36.98796	63.477	263.674	453
GOMX 1	334	20.3515	39.14	180.285	636
YAOGAN 29	522	47.83306	61.916	292.552	632
GLOBALSTAR M079	529	21.60443	79.771	205.448	1416
APRIZESAT 5	626	30.04942	29.449	179.673	688
IRIDIUM 136	1286	87.71908	32.554	352.763	785
SUSAT	1306	57.07354	7.509	211.847	374
CYGF05	1314	61.79961	14.582	122.095	522
⋮	⋮	⋮	⋮	⋮	⋮
SPEKTR R	332732	86.7313	2.537	92.876	327217

Table 4 represents a demonstrative output of a distance snapshot simulation, beaming from Barcroft to the Moon (Alt = 59.489° , Az = 180.742°), at 2018/02/01 midnight. The table (truncated for brevity) shows every active satellite, sorted by distance from the laser array. The distances reported are the distances from the center of the beam to the positions of satellites as calculated from their TLEs, not the worst-case minimum distances from the satellites to the edge of the beam. Using such simulations can be useful in determining optimal times to decide mission times and sites. In this particular example, the median distance between the DE beam and all satellites analyzed in this simulation was 8571.8 km.

5.3. Mars

In addition, for missions involving beaming to Martian based systems, simulations were made with a beaming duration of 3 months, with a beam diameter set at 10 km, and only considering active satellites. The results are tabulated in Table 5.

Table 5: Simulation: Mars.

Laser Array Base Site	t desired	t above 0°	t above 30°	No. Int.s	Int. duration	Int. Fraction
Barcroft Station	3 months	36.00 days	1.89 days	$535 \pm < 1$	$21.1 \pm < 0.1$ mins	4.07×10^{-4}
Atacama	3 months	50.35 days	32.81 days	$1207 \pm < 1$	$37.1 \pm < 0.1$ mins	5.11×10^{-4}
Haleakala	3 months	40.74 days	21.27 days	$688 \pm < 1$	$23.7 \pm < 0.1$ mins	4.04×10^{-4}
South Pole	3 months	90.00 days	0 days	$26284 \pm < 1$	$13.5 \pm < 0.1$ hours	6.24×10^{-3}

5.4. Pluto

Lastly, simulations for long-term DE mission scenarios to Pluto were also conducted. For these missions the beaming duration was set at 3 years, with a beam diameter set at 10 km, and only considering active satellites. The results are tabulated in Table 6.

Table 6: Simulation: Pluto.

Laser Array Base Site	t desired	t above 0°	t above 30°	No. Int.s	Int. duration	Int. Fraction
Barcroft Station	3 years	441.63 days	37.75 days	$3296 \pm < 1$	$2.06 \pm < 0.01$ hours	1.94×10^{-4}
Atacama	3 years	611.98 days	398.98 days	$4085 \pm < 1$	$2.06 \pm < 0.01$ hours	1.40×10^{-4}
Haleakala	3 years	497.78 days	262.33 days	$3079 \pm < 1$	$1.72 \pm < 0.01$ hours	1.44×10^{-4}
South Pole	3 years	1095.00 days	0 days	$45200 \pm < 1$	$24.8 \pm < 0.1$ hours	9.44×10^{-4}

As we can observe in Tabs. 3, 5, and 6, the probability of any active satellite intercepting with the beam is extremely small.

5.5. Beam Intercept Fraction

It was deemed appropriate to find the relationship between the total beaming duration and the proportion of time that the beam needed to be gated off. This allows us to establish whether the simulated data was consistent with our mathematical analysis.

As one can observe in Fig. 8, as the beaming duration increases, the beam intercept fraction for most simulations tends to approach the theoretical fraction we have calculated in Sec. 2 (marked by the dashed horizontal line). Each date was chosen such that the target would be within in the horizon of the beam, and as close to the epoch (2018/02/21) as possible. In the long term, as the beaming duration increases, initial

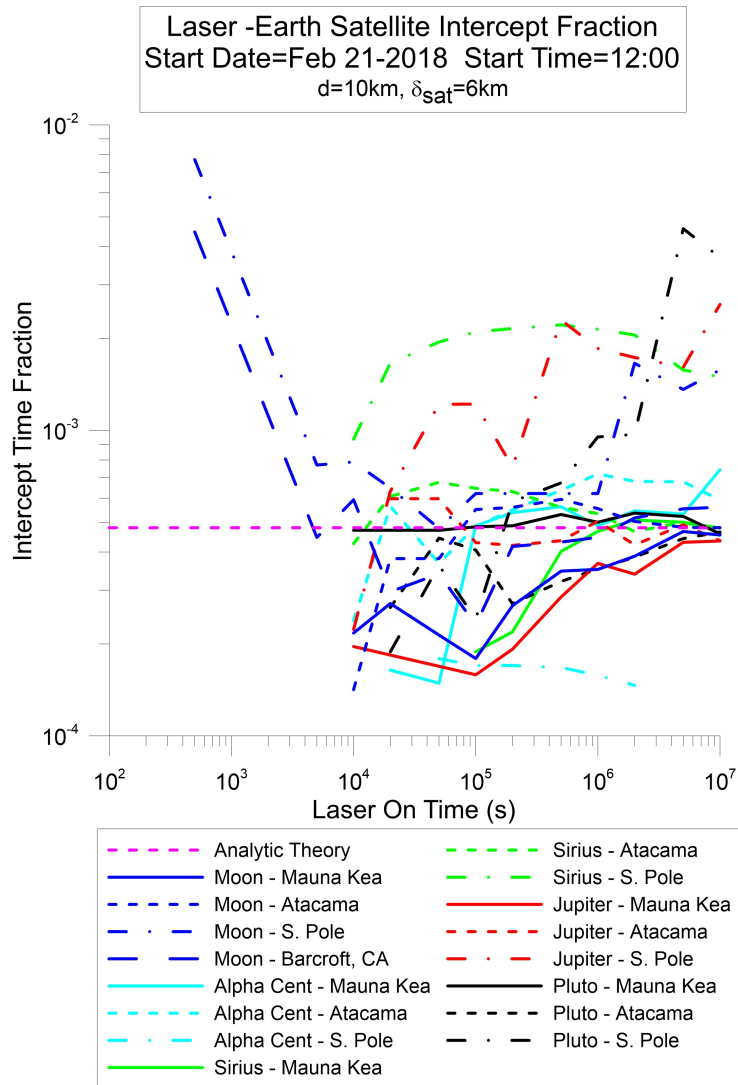


Figure 8: DE beam intercept fraction plotted against total beaming time for a different combinations of launch site and DE pointing target. The excess observed for the shorter durations is simply due to the combination of initial conditions and input arguments for the simulation. These included the initial beaming date, launch site, and target. Simulations performed at the South Pole exhibited higher incidences of satellite interception, due to intercepting more LEO satellites likely because of a horizon projection effect.

excess or absence of intercepts tends to average out to the analytical value.

We conclude that the average expected value of intercept fraction appears to be independent or weakly dependent on beaming duration and the launch site and target (except the South Pole tends to have a higher intercept fraction). As a result, we can conclude that it is indeed feasible to track a target in the sky for extended periods of time with negligible intercept time. This appears to hold true for all scenarios that were simulated. Although the beam may have to be gated off many times during the period of beaming in the long-term simulations (Mars, Moon, and Pluto), in general the interception time is very low, such that the beam can be turned on very shortly after the intercepting satellite has passed.

5.6. Sidelobe Intercepts

While the beam considered in this paper is assumed to be a single cylinder in profile, any real beam will have power outside this cylinder. This is often referred to as "sidelobe" structure. The detailed sidelobe structure will be important as the power levels are high enough that even relatively low level sidelobes need to be considered. For example a -30 db sidelobe with a 100 GW main beam is 100 MW which is still a major consideration for interception. The actual beam shape will depend on the specifics of the optical system and would need to be known in detail, though typical sidelobes are largely contained within the sub aperture beam size for a phased array. Since the satellites of interest are virtually all within the "near field" of the beam, this will lessen the problem. Once the detailed beam structure is known the same strategy used in this paper can be applied.

6. Discussion

Simulations of various DE mission scenarios of interest from multiple locations yielded results that are consistent with our analytical predictions. The intercept fraction as a function of beam time somewhat follows the law of large numbers and asymptotically approaches the worst-case analytical value of 4.9×10^{-4} for a 10 km array (see Eq. (22)). The median interception fraction is calculated to be 5.6×10^{-4} for all long

duration simulations. We expect that this value is higher than our worst-case estimate because we assumed the beam would point in the zenith direction at all times, and therefore take the minimum path length through the region of space occupied by satellites.

In general, missions from the South Pole yielded a longer beaming time above the horizon, but no beaming time above an altitude of 30° . Simulations at the South Pole also tended to have a higher intercept fraction, likely due to the targets being near its horizon (besides Alpha Centauri, which yielded a much lower intercept fraction). An orbital debris-debris collision avoidance system researched by NASA suggests laser sites closer to the poles for maximum targeting efficiency (Mason et al., 2011). Since we have the inverse goal, and as backed up by our simulations, it appears that beaming sites away from the poles would be better suited for our purposes.

6.1. Limitations

There are a number of limitations that must be considered during this study. Firstly, the full catalog of satellites only includes unclassified satellites, and hence all classified satellites are completely untracked by the simulation. Consequently, there may be intercepts with our beam that we do not expect if operating purely on TLE data from the Space Track database. However, this is unlikely to be a significant issue, as there is likely to be a relatively low number of these satellites compared to unclassified satellites. In addition, it is probable that in practice, when anticipating a real mission, the Laser Clearing House (LCH) would help us determine times where we may intercept a classified satellite, and therefore we would be able to take appropriate evasive action.

Secondly, as mentioned previously, the SGP4 orbit propagator is a simplified general perturbation model and has a number of inaccuracies. More recently, “specialized” propagators have been designed that use higher-order numerical integration with more detailed models of all known forces acting on a LEO object. For example, a specialized propagator, called SDP4, models the gravitational effects of the sun and moon, and specific sectoral and tesseral Earth harmonics which are important for half-day

and one-day period orbits (Kelso et al., 1988; Picone et al., 2005).

As alluded to previously, it is important to recognize that SGP4 accuracy, as the prediction date gets further from the epoch, decreases dramatically. In a study conducted by Osweiler, the range of errors encountered measuring normal and cross-track directions (normal to the plane defined by the current position and velocity vectors) using TLE and SGP4 was at most 0.25 km. However, the maximum velocity error was almost an order of magnitude greater at around 2 km after ten days. In order to be conservative we used the larger estimate of accuracy given by Vallado et al. (2006) and Rhodes (2015). These errors are greater when TLE's are used for satellites which experience significant amounts of drag (those with an orbital altitude of less than 800 km, i.e., LEO satellites (Osweiler, 2006)). Furthermore, the BSTAR term in the TLEs is sometimes underestimated by multiple orders of magnitude when there is even low solar activity, since SGP4 assumes an atmospheric model that does not vary with solar activity. However, this inaccuracy is likely to be much more severe for debris bodies, and must less so for satellites (Mason et al., 2011).

In addition, there are now even more accurate methods for orbital propagation. The state of the art methods for this use numerical integration with high-fidelity force models (for example high-order gravitational models). Accuracy is primarily a function of the force models that are included and how they are taken into account, as well as the orbital regime of the satellite. In regimes such as GPS, it is possible to obtain accuracy on the order of centimeters at the epoch, since force terms such as atmospheric drag become negligible.

The simulations do not take the elevation of the beaming sites into account, but rather assume that they are all at sea level. This assumption creates an inaccuracy in the relative positions of the beam and satellites, particularly if the location of the laser array is at high altitude and if the pointing altitude angle is low.

Furthermore, as mentioned previously, the accuracy of TLE-derived ephemeris de-

cays by 1–3 km a day and hence is only truly accurate a few days or a few weeks about the epoch of the particular TLE. This means that the long running simulations undertaken in this study (3 month, 1–3 year simulations) will not be accurate with regards to the ephemeris generation.

However, our research goal was not to obtain an extremely precise ephemeris for every satellite; the goal was to estimate general probabilities for interceptions, and to this end, the accuracies achieved by the SGP4 propagator and PyEphem more than suffice, since it is expected that the general distribution of satellites in space will not differ significantly, even in the long term. For future targeting systems and real mission scenarios, a similar program would require a means of dynamically updating the TLE to continuously correct for this accuracy decay while running (for example a targeting system for beaming power to the target (Finkleman, 2014)).

Lastly, our simulations do not take into account aircraft, which could also in theory intercept our beam. However, NASA has a Range Flight Safety program whose goal is to protect the safety and health of the public during operations. As proposed missions are under the NASA Innovative Advanced Concepts (NIAC) initiative, NASA Range Flight Safety would likely set up restricted airspace to avoid the area of the laser for the beaming duration (since aircraft can be rerouted unlike satellites (DeLoach, 2018)).

7. Conclusions

This paper has discussed simulations of pointing directed energy beams at targets in the sky, from a given location on the Earth, to thoroughly investigate the likelihood of Earth-orbiting spacecraft intercepting the beam and the duration of such intercepts.

A theoretical analysis using a simple physical model was performed a priori, in order to predict the intercept fraction, and this was calculated to be 3.9×10^{-4} .

Through simulations of various scenarios, using a wide range of input parame-

ters, such as beaming target, laser array site, beaming duration, and beam diameter, the results are consistent with this analysis. Indeed, it has been shown that there is a guarantee that we can find a window of time where there is exactly zero probability of intercepting an active Earth-orbiting satellite.

This research has widespread implications for the future of directed energy applications. We have shown it is feasible to point a directed energy beam at a celestial target for a wide range of durations, with negligible interception time with Earth-orbiting satellites. This opens up an array of possibilities for longer term DE mission proposals. In addition, accessible machinery now exists for future astronomers and others in the scientific community to predict satellite positions using TLE’s.

Acknowledgements

Funding for this program comes from NASA grants NIAC Phase I DEEP-IN 2015 NNX15AL91G and NASA NIAC Phase II DEIS 2016 NNX16AL32G and the NASA California Space Grant NASA NNX10AT93H as well as a generous gift from the Emmett and Gladys W. fund. PML acknowledges support as part of the advisory board and as part of the executive committee on Breakthrough Starshot.

Appendix A. NORAD Orbit propagator derivation

In this appendix, we outline the full derivation of the position and velocity vectors using the relevant TLE orbital parameters, as given by Kelso et al. (1988).

Appendix A.1. Physical and Mathematical Constants

The values of the physical and mathematical symbols used in the derivation that follows, are defined below. n_o , e_o , i_o , M_o , ω_o , Ω_o , \dot{n}_o , and \ddot{n}_o are all described by TLEs.

R_{\oplus} = The radius of Earth = 6378.135 km

n_o = the SGP type “mean” mean motion at epoch

e_o = the “mean” eccentricity at epoch

i_o = the “mean” inclination at epoch

M_o = the “mean” mean anomaly at epoch

ω_o = the “mean” argument of perigee at epoch

Ω_o = the “mean” longitude of ascending node at epoch

\dot{n}_o = the time rate of change of “mean” mean motion at epoch

\ddot{n}_o = the second time rate of change of “mean” mean motion at epoch

B^* = the SGP4 type drag coefficient

$k_e = \sqrt{GM}$ where G is Newton’s universal gravitational constant and M is the mass of the Earth

a_E = the equatorial radius of the Earth

J_2 = the second gravitational zonal harmonic of the Earth

J_3 = the third gravitational zonal harmonic of the Earth

J_4 = the fourth gravitational zonal harmonic of the Earth

$(t - t_o)$ = time since epoch

$$k_2 = \frac{1}{2}J_2a_E^2$$

$$k_4 = -\frac{3}{8}J_4a_E^4$$

$$A_{3,0} = -J_3a_E^3$$

q_o = parameter for the SGP4/SGP8 density function

s = parameter for the SGP4/SGP8 density function

$B = \frac{1}{2} C_D \frac{A}{m}$, the ballistic coefficient for SGP8 where C_D is a dimensionless drag coefficient and A is the average cross-sectional area of the satellite of mass m

Appendix A.2. SGP4 derivation

The SGP4 model uses the NORAD mean element sets described by TLE's. The original mean motion (n''_o) and semimajor axis (a''_o) are calculated by the following equations:

$$\begin{aligned} a_1 &= \left(\frac{k_e}{n_o} \right)^{\frac{2}{3}} \\ \delta_1 &= \frac{3}{2} \frac{k_2}{a_1^2} \frac{(3 \cos^2 i_o - 1)}{(1 - e_o^2)^{\frac{3}{2}}} \\ a_o &= a_1 \left(1 - \frac{1}{3} \delta_1 - \delta_1^2 - \frac{134}{81} \delta_1^3 \right) \\ \delta_o &= \frac{3}{2} \frac{k_2}{a_o^2} \frac{(3 \cos^2 i_o - 1)}{(1 - e_o^2)^{\frac{3}{2}}} \\ n''_o &= \frac{n_o}{1 + \delta_o} \\ n''_o &= \frac{a_o}{1 - \delta_o}. \end{aligned}$$

If the perigee of the orbit is between 98 km and 156 km, the value of s used in SGP4 is modified to be

$$s^* = a''_o(1 - e_o) - s + a_E$$

If the perigee is below 98 km, the value of s is modified to be

$$s^* = 20/R_{\oplus} + a_E.$$

If s is modified, then the value $(q_o - s)^4$ must be replaced by

$$(q_o - s^*)^4 = \left[[(q_o - s)^4]^{\frac{1}{4}} + s - s^* \right]^4.$$

Using the appropriate values of s and $(q_o - s)^4$, the following constants are calculated

$$\theta = \cos i_o$$

$$\begin{aligned}
\xi &= \frac{1}{a_o'' - s} \\
\beta_o &= (1 - e_o^2)^{\frac{1}{2}} \\
\eta &= a_o'' e_o \xi \\
C_2 &= (q_o - s)^4 \xi^4 n_o'' (1 - \eta^2)^{-\frac{7}{2}} \left[a_o'' \left(1 + \frac{3}{2} \eta^2 + 4e_o \eta + e_o \eta^3 \right) \right. \\
&\quad \left. + \frac{3}{2} \frac{k_2 \xi}{(1 - \eta^2)} \left(-\frac{1}{2} + \frac{3}{2} \theta^2 \right) (8 + 24\eta^2 + 3\eta^4) \right] \\
C_1 &= B^* C_2 \\
C_3 &= \frac{(q_o - s)^4 \xi^5 A_{3,0} n_o'' a_E \sin i_o}{k_2 e_o} \\
C_4 &= 2n_o'' (q_o - s)^4 \xi^4 a_o'' \beta_o^2 (1 - \eta^2)^{-\frac{7}{2}} \left(\left[2\eta(1 + e_o \eta) + \frac{1}{2} e_o + \frac{1}{2} \eta^3 \right] \right. \\
&\quad \left. - \frac{2k_2 \xi}{a_o'' (1 - \eta^2)} \left[3(1 - 3\theta^2) \left(1 + \frac{3}{2} \eta^2 - 2e_o \eta - \frac{1}{2} e_o \eta^3 \right) \right. \right. \\
&\quad \left. \left. + \frac{3}{4} (1 - \theta^2) (2\eta^2 - e_o \eta - e_o \eta^3) \cos 2\omega_o \right] \right) \\
C_5 &= 2(q_o - s)^4 \xi^4 a_o'' \beta_o^2 (1 - \eta^2)^{-\frac{7}{2}} \left[1 + \frac{11}{4} \eta(\eta + e_o) + e_o \eta^3 \right] \\
D_2 &= 4a_o'' \xi C_1^2 \\
D_3 &= \frac{4}{3} a_o'' \xi^2 (17a_o'' + s) C_1^3 \\
D_4 &= \frac{2}{3} a_o'' \xi^3 (221a_o'' + 31s) C_1^4.
\end{aligned}$$

The following equations account for long-term effects due to atmospheric drag and gravity

$$\begin{aligned}
M_{DF} &= M_o + \left[1 + \frac{3k_2(-1+3\theta^2)}{2a_o''^2 \beta_o^3} \right. \\
&\quad \left. + \frac{3k_2^2(13-78\theta^2+137\theta^4)}{16a_o''^4 \beta_o^7} \right] n_o'' (t - t_o) \\
\omega_{DF} &= \omega_o + \left[-\frac{3k_2(1-5\theta^2)}{2a_o''^2 \beta_o^4} + \frac{3k_2^2(7-114\theta^2+395\theta^4)}{16a_o''^4 \beta_o^8} \right. \\
&\quad \left. + \frac{5k_4(3-36\theta^2+49\theta^4)}{4a_o''^4 \beta_o^8} \right] n_o'' (t - t_o) \\
\Omega_{DF} &= \Omega_o + \left[-\frac{3k_2\theta}{a_o''^2 \beta_o^4} + \frac{3k_2^2(4\theta-19\theta^3)}{2a_o''^4 \beta_o^8} \right. \\
&\quad \left. + \frac{5k_4\theta(3-7\theta^2)}{2a_o''^4 \beta_o^8} \right] n_o'' (t - t_o)
\end{aligned}$$

$$\begin{aligned}
\delta\omega &= B^* C_3 (\cos \omega_o)(t - t_o) \\
\delta M &= -\frac{2}{3}(q_o - s)^4 B^* \xi^4 \frac{a_E}{e_o \eta} [(1 + \eta \cos M_{DF})^3 - (1 + \eta \cos M_o)^3] \\
M_p &= M_{DF} + \delta\omega + \delta M \\
\omega &= \omega_{DF} - \delta\omega - \delta M \\
\Omega &= \Omega_{DF} - \frac{21}{2} \frac{n_o'' k_2 \theta}{a_o''^2 \beta_o^2} C_1 (t - t_o)^2 \\
e &= e_o - B^* C_4 (t - t_o) - B^* C_5 (\sin M_p - \sin M_o) \\
a &= a_o'' [1 - C_1 (t - t_o) - D_2 (t - t_o)^2 - D_3 (t - t_o)^3 - D_4 (t - t_o)^4]^2 \\
\mathbb{L} &= M_p + \omega + \Omega + n_o'' \left[\frac{3}{2} C_1 (t - t_o)^2 + (D_2 + 2C_1^2)(t - t_o)^3 \right. \\
&\quad \left. + \frac{1}{4} (3D_3 + 12C_1 D_2 + 10C_1^3)(t - t_o)^4 \right. \\
&\quad \left. + \frac{1}{5} (3D_4 + 12C_1 D_3 + 6D_2^2 + 30C_1^2 D_2 + 15C_1^4)(t - t_o)^5 \right] \\
\beta &= \sqrt{1 - e^2} \\
n &= k_c \left| a \right|^{\frac{3}{2}}
\end{aligned}$$

where $(t - t_o)$ is the time that has elapsed from epoch. When the epoch perigee height is under 220 km, the equations for a and \mathbb{L} are truncated after the C_1 term, and terms involving C_5 , $\delta\omega$, and δM are ignored.

The long-period periodic terms are added

$$\begin{aligned}
a_{xN} &= e \cos \omega \\
\mathbb{L}_L &= \frac{A_{3,0} \sin i_o}{8k_2 a \beta^2} (e \cos \omega) \left(\frac{3 + 5\theta}{1 + \theta} \right) \\
a_{yNL} &= \frac{A_{3,0} \sin i_o}{4k_2 a \beta^2} \\
\mathbb{L}_T &= \mathbb{L} + \mathbb{L}_L \\
a_{yN} &= e \sin \omega + a_{yNL}.
\end{aligned}$$

Kepler's equation for $(E + \omega)$ is solved by defining

$$U = \mathbb{L}_T - \Omega$$

and using the iteration equation

$$(E + \omega)_{i+1} = (E + \omega)_i + \Delta(E + \omega)_i$$

with

$$\Delta(E + \omega)_i = \frac{U - a_{yN} \cos(E + \omega)_i + a_{xN} \sin(E + \omega)_i - (E + \omega)_i}{-a_{yN} \sin(E + \omega)_i - a_{xN} \cos(E + \omega)_i + 1}$$

and

$$(E + \omega)_1 = U.$$

Preliminary quantities needed for short-period periodics are calculated using the following equations.

$$e \cos E = a_{xN} \cos(E + \omega) + a_{yN} \sin(E + \omega)$$

$$e \sin E = a_{xN} \sin(E + \omega) - a_{yN} \cos(E + \omega)$$

$$e_L = (a_x N^2 + a_y N^2)^{\frac{1}{2}}$$

$$p_L = a(1 - e_L^2)$$

$$r = a(1 - e \cos E)$$

$$\dot{r} = k_e \frac{\sqrt{a}}{r} e \sin E$$

$$r \dot{f} = k_e \frac{\sqrt{p_L}}{r}$$

$$\cos u = \frac{a}{r} \left[\cos(E + \omega) - a_{xN} + \frac{a_{yN}(e \sin E)}{1 + \sqrt{1 - e_L^2}} \right]$$

$$\sin u = \frac{a}{r} \left[\sin(E + \omega) - a_{yN} - \frac{a_{xN}(e \sin E)}{1 + \sqrt{1 - e_L^2}} \right]$$

$$u = \tan^{-1} \left(\frac{\sin u}{\cos u} \right)$$

$$\Delta r = \frac{k_2}{2p_L} (1 - \theta^2) \cos 2u$$

$$\Delta u = -\frac{k_2}{4p_L^2} (7\theta^2 - 1) \sin 2u$$

$$\Delta \Omega = \frac{3k_2 \theta}{2p_L^2} \sin 2u$$

$$\begin{aligned}\Delta i &= \frac{3k_2\theta}{2p_L^2} \sin i_o \cos 2u \\ \Delta \dot{r} &= -\frac{k_2n}{p_L}(1 - \theta^2) \sin 2u \\ \Delta r\dot{f} &= \frac{k_2n}{p_L} \left[(1 - \theta^2) \cos 2u - \frac{3}{2}(1 - 3\theta^2) \right]\end{aligned}$$

The short-period periodics are added to produce the following osculating quantities

$$\begin{aligned}r_k &= r \left[1 - \frac{3}{2}k_2 \frac{\sqrt{1 - e_L^2}}{p_L^2} (3\theta^2 - 1) \right] + \Delta r \\ u_k &= u + \Delta u \\ \Omega_k &= \Omega + \Delta \Omega \\ i_k &= i_o + \Delta i \\ \dot{r}_k &= \dot{r} + \Delta \dot{r} \\ r\dot{f}_k &= r\dot{f} + \Delta r\dot{f}.\end{aligned}$$

Unit orientation vectors are then calculated by

$$\mathbf{U} = \mathbf{M} \sin u_k + \mathbf{N} \cos u_k$$

$$\mathbf{V} = \mathbf{M} \cos u_k - \mathbf{N} \sin u_k$$

where

$$\begin{aligned}\mathbf{M} &= \begin{pmatrix} M_x = -\sin \Omega_k \cos i_k \\ M_y = \cos \Omega_k \cos i_k \\ M_z = \sin i_k \end{pmatrix} \\ \mathbf{N} &= \begin{pmatrix} N_x = \cos \Omega_k \\ N_y = \sin \Omega_k \\ N_z = 0 \end{pmatrix}.\end{aligned}$$

Position is given by

$$\mathbf{r} = r_k \mathbf{U}$$

and velocity by

$$\dot{\mathbf{r}} = \dot{r}_k \mathbf{U} + (r\dot{f})_k \mathbf{V}.$$

References

- Bible, J., Johansson, I., Hughes, G.B., Lubin, P.M., 2013. Relativistic propulsion using directed energy, in: *Nanophotonics and Macrophotonics for Space Environments VII*, International Society for Optics and Photonics. p. 887605.
- Brashears, T., Lubin, P., Hughes, G.B., McDonough, K., Arias, S., Lang, A., Motta, C., Meinhold, P., Batliner, P., Griswold, J., et al., 2015. Directed energy interstellar propulsion of wafersats, in: *Nanophotonics and Macrophotonics for Space Environments IX*, International Society for Optics and Photonics. p. 961609.
- Brouwer, D., 1959. Solution of the problem of artificial satellite theory without drag. *The Astronomical Journal* 64, 378.
- Deloach, R., 2018. Nasa range flight safety program. URL: <https://kscsma.ksc.nasa.gov/RangeSafety/overview>.
- Finkleman, D., 2014. The dilemma of space debris. *American Scientist* 102, 26.
- Hou, L., Cai, Y., Liu, J., Hou, C., 2016. Variable fidelity robust optimization of pulsed laser orbital debris removal under epistemic uncertainty. *Advances in Space Research* 57, 1698–1714. URL: <https://doi.org/10.1016/j.asr.2015.12.003>, doi:10.1016/j.asr.2015.12.003. cited By 2.
- Hughes, G.B., Lubin, P., Griswold, J., Cook, B., Bozzini, D., O’Neill, H., Meinhold, P., Suen, J., Bible, J., Riley, J., et al., 2014. Optical modeling for a laser phased-array directed energy system, in: *Nanophotonics and Macrophotonics for Space Environments VIII*, International Society for Optics and Photonics. p. 922603.
- Kelso, T., Hoots, F., Roehrich, R., 1988. Spacetrack report no. 3-models for propagation of norad element sets.
- Kelso, T.S., 2017. Celestrak. URL: <https://celestrak.com/>.
- Kelso, T.S., 2018. Norad two-line element set format. URL: <https://www.celestrak.com/NORAD/documentation/tle-fmt.asp>.

- Lane, M.H., Hoots, F.R., 1979. General perturbations theories derived from the 1965 lane drag theory. Technical Report. Aerospace Defense Command Peterson AFB CO Office of Astroynamics.
- Lejba, P., Suchodolski, T., MichaÅek, P., Bartoszak, J., Schillak, S., ZapaÅnik, S., 2018. First laser measurements to space debris in poland. *Advances in Space Research* 61, 2609–2616. URL: <https://doi.org/10.1016/j.asr.2018.02.033>, doi:10.1016/j.asr.2018.02.033. cited By 0.
- Lubin, P., 2016. A roadmap to interstellar flight. *Journal of the British Interplanetary Society JBIS* 69, 40–72. URL: <http://arxiv.org/abs/1604.01356>.
- Mason, J., Stupl, J., Marshall, W., Levit, C., 2011. Orbital debris–debris collision avoidance. *Advances in Space Research* 48, 1643–1655.
- McKeon, B.P., 2016. Management of laser illumination of objects in space. URL: https://fas.org/irp/doddir/dod/i3100_11.pdf.
- Oswailer, V.P., 2006. Covariance estimation and autocorrelation of NORAD two-line element sets. Technical Report. Air Force Inst Of Tech Wright-Patterson AFB OH School Of Engineering And Management.
- Picone, J.M., Emmert, J.T., Lean, J.L., 2005. Thermospheric densities derived from spacecraft orbits: Accurate processing of two-line element sets. *Journal of Geophysical Research: Space Physics* 110. URL: <http://dx.doi.org/10.1029/2004JA010585>, doi:10.1029/2004JA010585. a03301.
- Rhodes, B., 2015. Standard general perturbation model 1.4. URL: <https://pypi.python.org/pypi/sgp4/>.
- Rhodes, B.C., 2008. Pyephem. URL: <http://rhodesmill.org/pyephem/>.
- Rovetto, R.J., Kelso, T., 2016. Preliminaries of a space situational awareness ontology. arXiv preprint arXiv:1606.01924 .
- Southwood, T., May, R., Hassell, M., Conway, G., 1974. Ecological strategies and population parameters. *The American Naturalist* 108, 791–804.

Vallado, D., Crawford, P., Hujsak, R., Kelso, T., 2006. Revisiting spacetrack report# 3, in: AIAA/AAS Astrodynamics Specialist Conference and Exhibit, p. 6753.

Wang, C., Zhang, Y., Wang, K., 2016. Impulse calculation and characteristic analysis of space debris by pulsed laser ablation. *Advances in Space Research* 58, 1854–1863. URL: <https://doi.org/10.1016/j.asr.2016.07.018>, doi:10.1016/j.asr.2016.07.018. cited By 3.